Acta Astronautica 94 (2014) 619–628

Contents lists available at ScienceDirect

Acta Astronautica

journal homepage: www.elsevier.com/locate/actaastro

Local debris congestion in the geosynchronous environment with population augmentation

Paul V. Anderson*, Hanspeter Schaub

Department of Aerospace Engineering Sciences, University of Colorado, 429 UCB, Boulder, CO 80309, USA

ARTICLE INFO

Article history:
Received 14 May 2013
Received in revised form
23 July 2013
Accepted 21 August 2013
Available online 13 September 2013

Keywords:
Geosynchronous orbit
Orbital debris
Debris forecasting

ABSTRACT

Forecasting of localized debris congestion in the geostationary (GEO) regime is performed to investigate how frequently near-miss events occur for each of the longitude slots in the GEO ring. The present-day resident space object (RSO) population at GEO is propagated forward in time to determine current debris congestion conditions, and new probability density functions that describe where GEO satellites are inserted into operational orbits are harnessed to assess longitude-dependent congestion in "business-as-usual" launch traffic, with and without re-orbiting at end-of-life. Congestion forecasting for a 50-year period is presented to illustrate the need for appropriately executed mitigation measures in the GEO ring. Results indicate that localized debris congestion will double within 50 years under current 80% re-orbiting success rates.

1. Introduction

The geostationary (GEO) ring is a unique commodity of the terrestrial satellite industry that is becoming increasingly contaminated with orbital debris [12,14,27]. As the lack of atmospheric drag effects at the GEO altitude renders the lifetimes of these debris infinitely long [13,16,28], conjunction and mitigation assessment must be performed to safeguard operational GEO satellites from colliding with the debris population. As GEO satellites must maintain a specific longitude—and cannot simply phase shift to evade debris—analysis of the *macroscopic* behavior of the GEO debris population is required to describe debris fluxes through particular GEO longitude slots, to forecast how frequently operational assets in these regions must potentially perform maneuvers to mitigate conjunctions. Rather than presenting a high-precision analysis required for risk assessment and mitigation, this study builds upon the analysis of Anderson and Schaub [1], who illustrate a 1-year, macroscopic congestion forecast for debris at GEO, to determine which *localized* regions of the GEO ring are, in general, most susceptible to rising debris fluxes at different times. In contrast to this earlier work, this paper presents non-homogeneous methods for modeling GEO satellite growth, providing for longer-term congestion forecasting. As overcrowding of GEO is becoming a serious concern for satellite owners and operators internationally, knowledge of debris flux patterns—termed debris weather—is an imperative for space situational awareness activities at GEO.

Fig. 1 illustrates the unclassified, trackable resident space object (RSO) population at GEO (e.g., controlled assets and uncontrolled debris larger than approximately 1 m in diameter) for which up-to-date tracking data were available as of January 1, 2013. Following Flohrer [7], this population is subdivided into four primary classes, as is discussed in Section 2: (1) fully controlled assets with E-W and/or N-S station-keeping capability, (2) drifting objects that circulate along the GEO ring, as seen by an Earth-fixed observer, (3) librating objects that are trapped within one or both of the potential wells located at 75°E and 105°W, and (4) indeterminate objects, for which the type of orbit is unclassifiable or unknown. Each of these classes contributes uniquely to longitude-dependent debris weather at GEO, leading to non-uniform congestion patterns in the Earth-fixed frame [1].

* Corresponding author. Tel.: +1 5869099422.
E-mail addresses: paul.anderson@colorado.edu (P.V. Anderson), hanspeter.schaub@colorado.edu (H. Schaub).

0094-5765/$ - see front matter © 2013 IAA. Published by Elsevier Ltd. All rights reserved.
http://dx.doi.org/10.1016/j.actaastro.2013.08.023

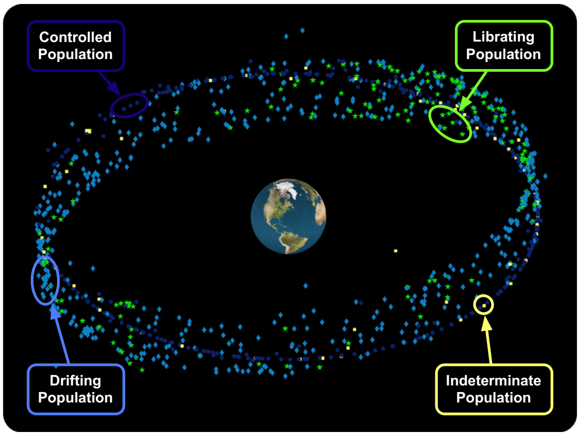

Fig. 1. Distribution of GEO RSO population on 01/01/13.

Existing debris analysis and evolution software [2,17,18] use intertially-fixed cell definitions to track debris cell passage events (CPE) arising from osculating orbit intersections with the cells of interest during long-term propagation. With the assistance of various probability models, the associated spatial density and flux contributions for each CPE may thereafter be computed and implemented in collision risk assessment. For the GEO regime, these analysis tools often average over cell right ascension, providing debris fluxes as a function of altitude and declination [16]. Furthermore, employing inertially-fixed cell definitions only, flux contributions to particular GEO longitude slots at arbitrary times cannot be determined. Thus, although spatially-averaged flux conditions at GEO may be estimated with this software, local intersection events for arbitrary longitude slots are not accessible, and the latter is of significant interest to space operators concerned with the debris conditions in the vicinity of a functioning satellite. Furthermore, McKnight and Di Pentino [20] emphasize that fluxes averaged across longitude and time can grossly misrepresent short-term collision hazard, and as a consequence, alternative GEO collision hazard depictions that employ higher temporal and spatial resolutions should be adopted by the operator community. Chrystal et al. [5] illustrate that the gravitational wells at GEO render the average flux a less relevant statistic for evaluating congestion at GEO, as the probability of collision at the center of these wells is seven times larger than at longitudes far from these regions.

Following Anderson and Schaub [1], this study implements a toroidal cell configuration at the GEO altitude to evaluate the impact of the current RSO population—augmented under representative launch traffic models during long-term propagation—on each of the longitude slots at GEO, by performing a *near-miss analysis* that attempts to assess the frequency at which uncontrolled objects pass within a given distance of a particular longitude slot. To enhance intuition, an integer number of near-miss events is used here as the alternative to typical spatial density and flux metrics [16]. Population augmentation in the GEO ring has been investigated briefly in the literature [16,27], albeit, these studies present debris fluxes averaged across longitude, altitude, and time, and therefore fail to address which longitude slots are the most prone to proliferating debris populations at GEO. This paper addresses this void in the literature by predicting longitudes of high-risk placement for operational GEO assets for the next 50 years, serving to further enforce that the averaging of debris densities and fluxes is becoming increasingly misrepresentative for the GEO regime.

Local congestion forecasting at GEO is an imperative activity—it provides a metric as to how frequently satellite operators with assets in particular longitude slots will have to track nearby debris motion and consider avoidance maneuvers. The latter is of a particular importance, as avoidance maneuvers can temporarily force a satellite outside of its longitude slot, which may pose problems for the mission, and be difficult to manage if neighboring satellites are collocated in the same slot. Currently, the RSO population at GEO is sparse enough such that a simple time-shift of a scheduled maintenance maneuver is sufficient for evading debris. In these situations, no additional propellant is expended beyond that allocated for routine GEO station-keeping. However, as the debris population at GEO continues to increase, the amount of propellant required to maintain a specified longitude slot while simultaneously executing avoidance maneuvers—and the costs associated with analyzing conjunction events to determine if evasive action is even necessary—will begin increasing, as well. The objective of this paper is to illustrate worst-case debris congestion at GEO under representative launch traffic alone for a 50-year prediction period, and demonstrate that mitigation measures at end-of-life can serve to attenuate localized congestion, especially in the neighborhoods of the Eastern and Western gravitational wells.

It is important to emphasize that nominal launch events are the only input to the debris growth model implemented in this study. Explosion events, on-orbit collisions, ejection of solid rocket motor (SRM) slag, shedding of multi-layered insulation (MLI), and other debris growth mechanisms considered in Wegener et al. [27], for example, are not treated in this analysis. Although future work will address the impact of explosion and collision events occurring in the GEO environment, the focus of this study is to provide a conservative lowerbound for the true debris weather situation occurring in the GEO ring.

2. Current RSO population at GEO

The RSO population in the GEO ring is classified with a taxonomy used by the European Space Agency's DISCOS database (Database and Information System Characterising Objects in Space) [7]. For GEO RSOs, seven orbit categories are used to classify the type of orbits traversed by these objects. Table 1 provides a description of this classification system; note that only uncontrolled objects are assumed to contribute to local debris congestion in this study. GEO RSOs are selected according to the requirements imposed in the *Classification of Geosynchronous Objects* reports [7]:

- Eccentricity smaller than 0.2 ($e < 0.2$)
- Inclination smaller than 70° ($i < 70^\circ$)

Table 1
Orbit classifications for geosynchronous objects used in GEO congestion study.

Class	Type	Description
C1	Controlled	Longitude/inclination control (E-W/N-S control)
C2	Controlled	Longitude control only (E-W control only)
D	Drifting	Drift above/below/through protected GEO zone
L1	Librating	Libration about Eastern stable point ($\lambda = 75°$E)
L2	Librating	Libration about Western stable point ($\lambda = 105°$W)
L3	Librating	Libration about Eastern/Western stable points
IN	Indeterminate	Unknown status (e.g., recent TLE not available)

- Mean motion between 0.9 and 1.1 revolutions per sidereal day ($0.9 < n < 1.1$)[1]

Orbital data are obtained from publicly available two-line element (TLE) sets provided by U.S. Strategic Command (USSTRATCOM).[2] For this debris study, a reference TLE set obtained on 01/01/13 is employed; the class distribution for the 1122 objects extracted from this set is illustrated in Fig. 2. TLE data are provided as doubly-averaged Keplerian elements [16] with mean motion instead of semi-major axis, transformed into Cartesian states in the true equator, mean equinox (TEME) frame [25] via SGP-4 theory [10] for this study.[3] Note that because of the limited accuracy of the TLE sets, these data are not intended for high-precision analyses —as the purpose of this study is to forecast near-miss events occurring on a macroscopic scale, and investigate first-order growth of the localized debris congestion at GEO, the accuracy of these data is sufficient.[4] Furthermore, as only objects larger than approximately 1 m are routinely tracked at the GEO altitude [7], only RSOs at least of this size are considered here. Since this study only incorporates the trackable, catalogued, and unclassified GEO RSOs with up-to-date TLEs, the findings of this study serve to illustrate a conservative lower bound of the true debris congestion situation in the GEO regime. Future work will address the impact of on-orbit collision and fragmentation events on the longitude slots at GEO.

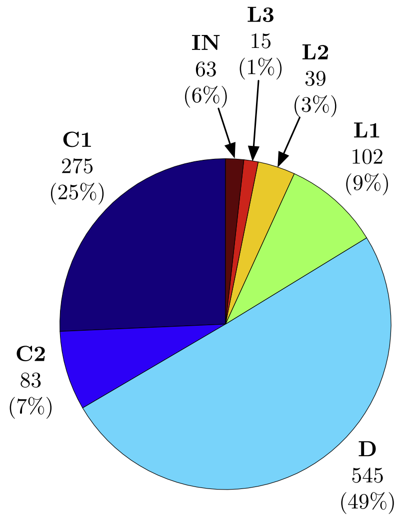

Fig. 2. Distribution of GEO RSO population.

3. Forecasting local GEO congestion

3.1. Formulation of near-miss events

Near-miss events for the GEO longitude slots are determined by formulating a GEO-encompassing torus of major radius $r_{GEO} = 42\,164$ km and minor radius $\tilde{r}$, partitioned into longitude increments of $\Delta\lambda = 1.0°$ [1]. The minor radius $\tilde{r}$ is equivalent to the radius of the circular torus cross-section, and provides a means to evaluate debris congestion levels occurring within various distances of the GEO longitude slots; a larger minor radius captures more near-miss CPE. Minor radii of $\tilde{r} = 50/100/300/700$ km are simulated to evaluate the frequency of near-miss CPE occurring from distances representative of a 1° longitude slot at GEO (~ 700 km) to distances at which precise conjunction assessment could potentially be considered (~ 50 km). Further, this torus formulation is a natural choice for evaluating CPE for the non-inertial GEO slots, as the torus geometry is invariant as seen by both the inertial frame (i.e., MJ2000) and Earth-centered, Earth-fixed frame, in which the GEO longitude slots are fixed [1].

Near-miss events are detected during propagation of an object by checking for the transversal of this GEO torus boundary at each time step during numerical integration. Mathematically, a near-miss event occurs if [1]

$$\left(r_{GEO} - \sqrt{r_X^2 + r_Y^2}\right)^2 + r_Z^2 - \tilde{r}^2 < 0 \tag{1}$$

is satisfied, where $(r_X, r_Y, r_Z)^T$ is the RSO position vector expressed in the inertial frame. The longitude of intersection λ_{CPE} is thus determined as

$$\lambda_{CPE} = \arctan\left(\frac{r_Y}{r_X}\right) - \alpha_G \tag{2}$$

where α_G is the right ascension of Greenwich (Greenwich sidereal time) [6]. When a torus-intersection is detected with Eq. (1), the longitude of intersection is determined with Eq. (2), and the total near-miss count for the corresponding toroidal cell is updated. To ensure that equivalent intersection events are not accounted for more than once

[1] This mean motion range corresponds to the semi-major axis range [−2596, 3068] km with respect to the GEO radius. Although RSOs that can be classified as geosynchronous (albeit loosely) may exist outside of this interval, they are not considered in this study, as the torus introduced in Section 3.1 to analyze GEO congestion only extends to 700 km in minor radius. Results are therefore dominated by the mean motion range $0.98 < n < 1.03$.

[2] Publicly available TLE data sets (updated twice daily) are available for bulk download from: https://www.space-track.org/.

[3] ANSI-C implementation of merged SGP-4/SDP-4 theory for TLE processing is available from: http://www.sat.dundee.ac.uk/~psc/sgp4.html [26].

[4] Numerical justification for the use of TLE data as a state source is given in Section 3.2.

during CPE checking, counting logic is employed before a cell intersection counter is updated to screen the event for redundancy. The full algorithm for determining near-miss events with the torus formulation is detailed by Anderson and Schaub [1].

3.2. Propagator and implementation

A special perturbations propagation routine implemented in ANSI-C and parallelized with the OpenCL architecture is implemented to propagate the uncontrolled GEO population and determine torus intersection events. Per implementation considerations of the OpenCL configuration,[5] a lower-fidelity, albeit representative force model of the GEO environment is implemented, with the added benefit of dramatically decreased simulation run times. Here, the two-body equations of motion are numerically integrated under a 4×4 EGM-96 spherical harmonics expansion, luni-solar perturbations, and solar radiation pressure (SRP), modeled with the cannonball assumption described by Vallado [25], and harshly attenuated with the geometric occultation algorithm presented by Montenbruck and Gill [21]. The equations of motion are thus written as

$$\ddot{\boldsymbol{r}} = -\frac{\mu_\oplus}{r^3}\boldsymbol{r} + \boldsymbol{a}_\oplus + \boldsymbol{a}_{☾} + \boldsymbol{a}_\odot + \boldsymbol{a}_{\mathrm{SRP}} \tag{3}$$

where the first term denotes Keplerian two-body acceleration, $\boldsymbol{a}_\oplus$ is the acceleration due to the nonsphericity of Earth, $\boldsymbol{a}_{☾}$ and $\boldsymbol{a}_\odot$ are the third-body contributions from the Moon and Sun, respectively, and $\boldsymbol{a}_{\mathrm{SRP}}$ is the SRP acceleration. SRP is modeled using the inverse-square diffusion formulation of the solar luminosity $L_\odot \approx 3.839\times10^{26}$ J/s, with coefficient of reflectivity $c_r \equiv 1.5$ and GEO-representative area-to-mass ratio $A_\odot/m = 0.04\ \mathrm{m}^2/\mathrm{kg}$.[6] Although variations exist in $A_\odot/m$ within the class of objects considered, Anderson and Schaub [1] illustrate that with such a small value for $A_\odot/m$, SRP has a negligible effect on the GEO congestion patterns similar to those presented later in this paper. High area-to-mass ratio (HAMR) objects are more susceptible to $A_\odot/m$ variations, but are not treated in the current study.

In higher-fidelity force models, coordinate transformations between Earth-fixed and Earth-inertial frames utilize accurate Earth orientation parameters to account for precession, nutation, and polar motion; software suites such as the SPICE toolkit can be used to perform these complex coordinate transformations.[7] In this parallelized propagator, however, a lower-fidelity transformation that accounts strictly for a z-axis rotation by Greenwich sidereal time is used for purposes of increased speed at run time. Furthermore, instead of drawing the inertial Moon and Sun position vectors from the ephemerides, this routine implements low-precision formulae for the geocentric coordinates of these bodies, as provided in the 2013 *Astronomical Almanac* [24]. Since the focus of this study is to illustrate general congestion patterns at GEO—and not provide precision predictions—these assumptions provide appropriate fidelity for the purposes of this paper, as is shown below.

The propagator utilizes an eighth-order, predictor–corrector Gauss–Jackson integrator [3] initialized with the Prince–Dormand 8(7) algorithm for integration of the equations of motion in Eq. (3). During initial propagation of the debris population to the near-miss event start date, and during near-miss computations in the prediction span, a time step of 10 min is specified for sufficient fidelity in capturing macroscopic congestion trends. Simulation results change insignificantly when smaller steps are used.

To validate this lower-fidelity, parallelized propagation routine, near-miss events for a $\tilde{r} = 700$ km torus through a 5-year interval (using the baseline RSO population provided in the 01/01/13 reference TLE set) are computed for both this propagator and a higher-fidelity, sequential propagator.[8] The debris weather forecast for this 5-year interval is illustrated in Fig. 3(a) and (b) for the higher-fidelity, sequential propagation and lower-fidelity, parallel propagation, respectively. Run time for lower-fidelity, parallel propagation is 4.5 min, orders-of-magnitude faster than the approximate 9.5 h required for the higher-fidelity, sequential propagation with the SPICE toolkit. More importantly, however, is that macroscopic debris weather patterns predicted by these propagation methods differ insignificantly—reduced-fidelity, parallel propagation is thus harnessed for the dramatic speed increase it gives.

It is interesting to quantify the sensitivity of this near-miss torus intersection metric to uncertainties present in TLE data. Flohrer et al. [8] utilize the European Space Agency's orbit determination tool ODIN to assess TLE orbit errors and estimate covariance information for various regimes. Based on the analysis of 886 GEO TLE sets for the snapshot epoch January 1, 2008, Flohrer et al. [8] determine that the standard deviations for the uncertainties in the radial, in-track, and cross-track directions are 0.359 km, 0.432 km, and 0.086 km, respectively, for the GEO regime. Therefore, the 5-year, parallel propagation is repeated to account for these TLE position uncertainties, i.e., the radial, in-track, and cross-track coordinates of each GEO object are perturbed by normally distributed random numbers with a mean of zero and associated standard deviation as specified above. Fig. 3(c) illustrates that this artificial discrepancy in the initial conditions does not have an impact on the macroscopic congestion patterns observed. The torus intersection metric used to quantify near-miss events is thus insensitive to inherent TLE uncertainties, unless torus minor radii less than 5–10 km are to be considered.

4. Congestion forecasting with population augmentation

4.1. Operational GEO orbit model

During long-term congestion forecasting, the GEO RSO population must be meaningfully augmented to simulate

[5] The *OpenCL 1.2 Specification* is available from Khronos Group at: http://www.khronos.org/registry/cl/.

[6] Schaub and Jasper [23] indicate that this ratio is representative for operational and defunct satellites at GEO; this value is thus used in the SRP computation for all RSOs.

[7] The Jet Propulsion Laboratory's (JPL) SPICE toolkits are available from: http://naif.jpl.nasa.gov/naif/toolkit.html.

[8] This higher-fidelity propagator uses an equivalent Gauss–Jackson integration routine with a 5-min time step, accounts for precession, nutation, and polar motion during 8×8 gravity evaluation, and draws the third-body position vectors from the DE421 ephemeris.

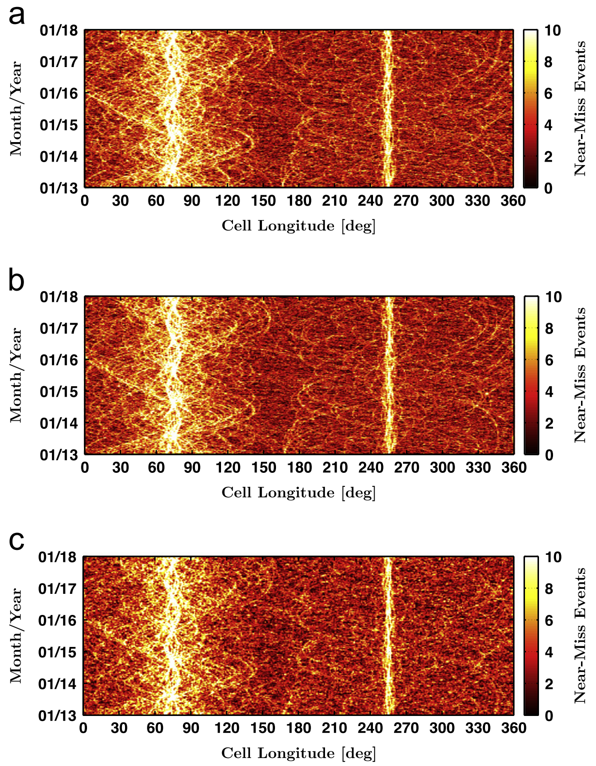

Fig. 3. 5-year propagator and force model comparison ($\tilde{r} = 700$ km). (a) Near-miss CPE for 700 km GEO torus (sequential propagation), (b) near-miss CPE for 700 km GEO torus (parallel propagation) and (c) near-miss CPE for 700 km GEO torus, accounting for position uncertainties in TLE sets.

nominal launch traffic for this regime. Realistic population augmentation requires an operational GEO orbit model to quantify *where* new GEO satellites are typically positioned at insertion into their designated longitude slots – such a model serves to generate the initial conditions for new controlled satellites created during the long-term forecasting (the GEO launch instantiation procedure is outlined in Section 4.2). To construct a first-order operational orbit model, data from the 01/01/13 reference TLE set, the *Space-Track Geosynchronous Report*,[9] and the electronic *SatBeams* database[10] are compiled, yielding semi-major axis, eccentricity, inclination, and geocentric longitude information for 768 past and present GEO satellites (including all unclassified launches to GEO as of 01/01/13), and 94 satellites planned through the year 2020. Employing these data, stacked histograms are generated for the semi-major axis, eccentricity, inclination, and geocentric longitude, and appropriate probability density functions are fit to these histograms to construct representative distributions from which the orbital elements of a new controlled satellite may be drawn.[11] Fig. 4 shows these parameter histograms (stacked by launch decade) and their associated density functions, summarized for each element below:

- *Semi-major axis* (a): Normal distribution with mean $\mu = 42164.8$ km and standard deviation $\sigma = 1.0$ km. The probability density function (PDF) and cumulative distribution function (CDF) for this distribution are given by (for $-\infty < x < \infty$)

$$f_{\mathcal{N}}(x;\mu,\sigma) = \frac{1}{\sigma\sqrt{2\pi}}\exp\left[-\frac{1}{2}\left(\frac{x-\mu}{\sigma}\right)^2\right] \tag{4}$$

$$F_{\mathcal{N}}(x;\mu,\sigma) = \frac{1}{2}\left[1+\operatorname{erf}\left(\frac{x-\mu}{\sigma\sqrt{2}}\right)\right] \tag{5}$$

- *Eccentricity* (e): Half-normal distribution derived from normal distribution with $\sigma = 5.0\times10^{-4}$, for which the PDF and CDF are given by (for $x \geq 0$)

$$f_{\mathcal{N}/2}(x;\sigma) = \frac{\sqrt{2}}{\sigma\sqrt{\pi}}\exp\left(-\frac{x^2}{2\sigma^2}\right) \tag{6}$$

$$F_{\mathcal{N}/2}(x;\sigma) = \operatorname{erf}\left(\frac{x}{\sigma\sqrt{2}}\right) \tag{7}$$

- *Inclination* (i): Half-normal distribution derived from normal distribution with $\sigma = 0.08^\circ$.
- *Longitude* (λ): Gaussian mixture of two wrapped normal distributions with $(\mu_1,\sigma_1) = (55^\circ, 65^\circ)$ and $(\mu_2,\sigma_2) = (260^\circ, 25^\circ)$, mixed as follows[12]:

$$\lambda \sim 0.75 f_{\mathcal{W}}(\mu_1,\sigma_1) + 0.25 f_{\mathcal{W}}(\mu_2,\sigma_2) \tag{8}$$

where the PDF and CDF for the wrapped normal distribution are given by (for $0 \leq x < 2\pi$)

$$f_{\mathcal{W}}(x;\mu,\sigma) = \frac{1}{\sigma\sqrt{2\pi}} \times \sum_{k=-\infty}^{\infty} \exp\left[-\frac{(x-\mu+2\pi k)^2}{2\sigma^2}\right] \tag{9}$$

$$F_{\mathcal{W}}(x;\mu,\sigma) = \frac{1}{2}\sum_{k=-\infty}^{\infty}\left[\operatorname{erf}\left(\frac{x-\mu+2\pi k}{\sigma\sqrt{2}}\right) - \operatorname{erf}\left(\frac{-\mu+2\pi k}{\sigma\sqrt{2}}\right)\right] \tag{10}$$

For computer implementations, sampling from the distributions is performed by drawing a pseudo-random number on the interval $[0,1]$ that represents the cumulative probability in the desired distribution. The appropriate CDF is then back-solved for the value of x that would yield this cumulative probability. Back-solving the wrapped normal CDF is performed by incrementally stepping through the interval $x \in [0, 2\pi]$ in Eq. (10) until the value of the random number has been achieved to tolerance (it is sufficient to iterate k as $k = -100\ldots100$).

Right ascension of the ascending node is selected uniformly on the interval $\Omega \in [0, 360^\circ]$, and the true anomaly is

[9] The Space-Track Geosynchronous Report is available at: https://www.space-track.org/perl/geo_report.pl.

[10] The SatBeams database provides GEO satellite longitude and launch year data, and is available at: http://www.satbeams.com/satellites.

[11] Under this methodology, the semi-major axis, eccentricity, inclination, and longitude of the new controlled satellite are assumed to be independent and uncorrelated parameters.

[12] A Gaussian mixture is implemented to simulate the bimodality of the longitude histogram in Fig. 4(d), i.e., high concentrations of operational satellites above Europe/Asia and North America, but minimal assets above the Atlantic and Pacific Oceans.

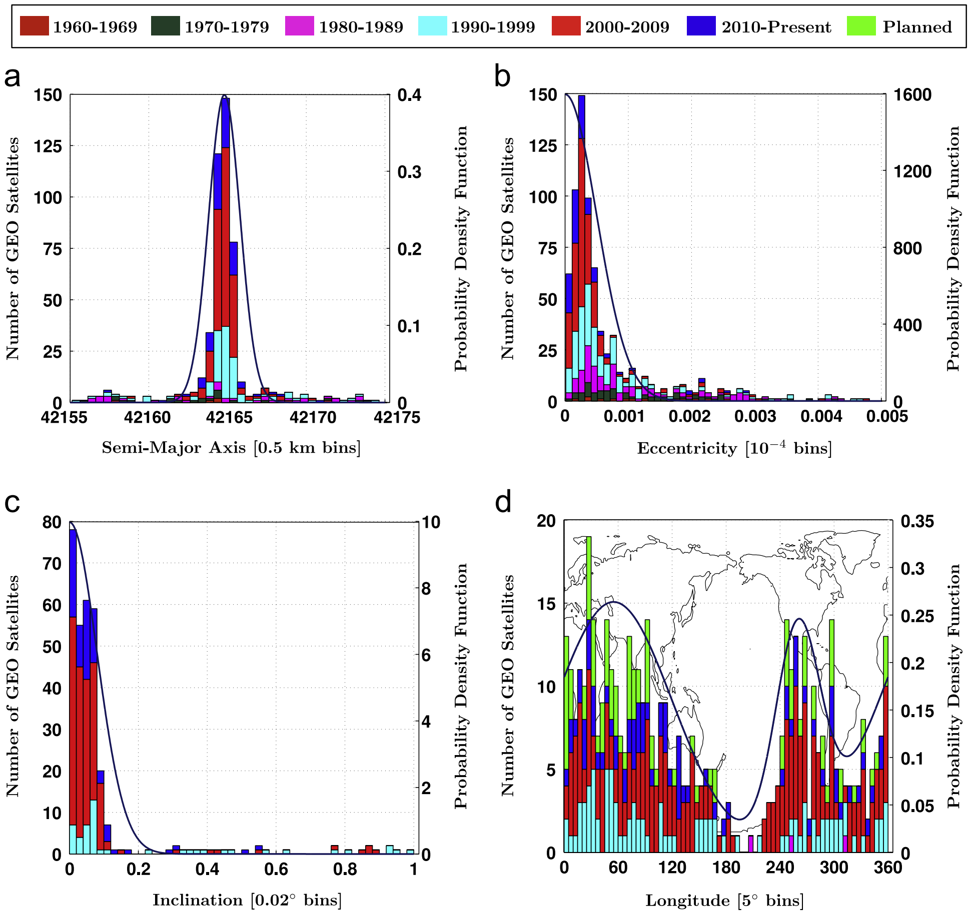

Fig. 4. Parameter distributions for representative sampling of operational GEO orbits. (a) Semi-major axis PDF for GEO orbit, (b) eccentricity PDF for GEO orbit, (c) inclination PDF for GEO orbit and (d) longitude PDF for GEO orbit.

initialized as 0°, i.e., new satellites are inserted at the perigee of their operational orbits. Therefore, the argument of perigee ω must satisfy

$$\omega = \alpha_G + \lambda - \Omega \tag{11}$$

where α_G denotes the right ascension of Greenwich, computed at the epoch of insertion. After the initial orbit elements have been sampled in this manner, these Keplerian elements are converted into a Cartesian state and assigned to the new satellite. This methodology ensures that new controlled satellites created during long-term forecasting exhibit initial orbital elements that are highly representative of the operational GEO orbits harnessed since the first GEO utilization in 1963.

4.2. Business as usual without mitigation

Launches to operational GEO orbits are simulated with the probabilistic, open-loop event instantiation method implemented in the European Space Agency's DELTA (Debris Environment Long-Term Analysis) tool [16]. Following Klinkrad [16], the probability $\mathcal{P}_j$ of j launches occurring in a given analysis interval is modeled with the Poisson distribution

$$\mathcal{P}_j = \frac{c^j}{j!} \exp(-c) \tag{12}$$

where the parameter c is the average number of launches occurring during the analysis interval, computed as $c=$ (average annual launch rate to orbit regime [years^{-1}]) $\times$ (length of analysis interval [years]) [16]. Assuming the “business-as-usual” GEO launch rate of 30 satellites per year [16,27] and using 1-day analysis intervals, $c \approx 0.082$ as a first approximation for typical launch traffic at GEO. For computer implementations, the probabilities $\mathcal{P}_j$ for $j = 0, 1, \ldots, k$ are first determined until a threshold ε is achieved, such that $\mathcal{P}_{k+1} \le \varepsilon$ (for this study, $\varepsilon \equiv 10^{-6}$). The resultant probabilities are then normalized such that their sum is equal to 1:

$$\hat{\mathcal{P}}_j = \frac{\mathcal{P}_j}{\sum_{i=0}^{k} \mathcal{P}_i} \Longrightarrow \sum_{j=0}^{k} \hat{\mathcal{P}}_j = 1 \tag{13}$$

A pseudo-random number $\hat{\zeta}$ on the interval [0, 1] is drawn, and the number of launch occurrences in the analysis interval is thus determined by the largest j for which the sum of the normalized probabilities $\hat{\mathcal{P}}_j$ is still less

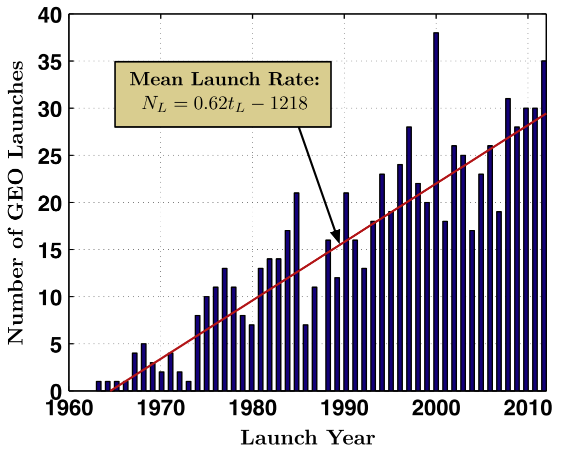

Fig. 5. Number of launches to operational GEO orbits by launch year.

than $\hat{\zeta}$, i.e.,

$$\sum_{i=0}^{j} \hat{\mathcal{P}}_i \le \hat{\zeta} < \sum_{i=0}^{j+1} \hat{\mathcal{P}}_i \tag{14}$$

Therefore, following each day of propagation, a pseudo-random number $\hat{\zeta}$ is drawn, and the number of launches during the past day is determined with Eq. (14). If a successful launch has been initiated, a controlled GEO satellite (C1) is created, and the initial orbit elements are sampled from the representative distributions presented in Section 4.1. For the purposes of this congestion study, the satellite is injected into its orbit at midnight, and it is assigned a nominal lifetime of 15 years.[13] Controlled satellites that achieve end-of-life (EOL) during propagation are deactivated without any re-orbiting attempt—these satellites are labeled as indeterminate (IN) and added to the uncontrolled RSO population for propagation.

Although the "business-as-usual" launch rate of 30 new GEO satellites per year offers a suitable first approximation for long-term congestion forecasting in this arena, it is more instructive to consider the more realistic case of an increasing launch rate to operational orbits at GEO. Fig. 5 illustrates the number of launches to GEO occurring each year since 1963, harnessing data compiled from the *Space-Track Geosynchronous Report*. Observing that the number of launches N_L is approximately proportional to the launch year t_L, linear regression provides the following linearly increasing GEO launch traffic model:

$$N_L = 0.62t_L - 1218 \quad \text{[launches/year]} \tag{15}$$

To implement this launch traffic model, the parameter c is updated after every year of propagation, and the probabilities in Eqs. (12)–(14) are recomputed to reflect a linearly increasing launch rate. Fig. 6 illustrates local congestion for the 01/13–01/63 prediction span, assuming this "business-as-usual" model in the absence of mitigation measures. Fig. 6(a) illustrates the absolute number of near-miss events per day for the 50 km GEO torus, while Fig. 6(b) quantifies increase in the mean number of near-miss events per day—averaged over each year of propagation—over the idealized "no future launches" traffic scenario (similar results are illustrated in Fig. 6 for the 100/300/700 km minor radius cases). As anticipated, the strength of the debris weather is amplified with the torus radius $\tilde{r}$, and localized congestion in the vicinity of the Eastern and Western gravitational wells dramatically expands as propagation time progresses.[14] The accumulation of uncontrolled objects around these gravitational wells is a well-known result, as discussed by Luu and Sabol [19] and Chobotov [4], for example. This is a particularly troublesome notion, as operating GEO satellites are typically inserted into longitude slots near these problematic regions—studying Fig. 4(d), it is evident that the two modes of the bimodal PDF selected for the geocentric longitude distribution are located directly over these two regions of maximum congestion, illustrated in Fig. 6. Assets residing in the longitude interval $\lambda \in (60^\circ, 90^\circ)$ around the Eastern gravitational well could be subjected to upwards of 30 additional near-miss events *per day* at 700 km, on an average, by the year 2063. At a distance of a mere 50 km, Fig. 6 predicts that assets near both stable points could experience upwards of 10 near-misses daily by 2063. These are striking outcomes that begin to corroborate the hypothesis that as the debris population in the GEO regime continues to rise unchecked, the amount of propellant required for routine station-keeping will rise in tandem, to account for the increasing frequency of potential collision avoidance maneuvers. Further, this result has significant implications for satellite insurance in high-risk longitude slots, and rising costs associated with determining whether or not execution of a collision avoidance maneuver is necessary in the first place. Again, as uncontrolled debris objects smaller than 1 m—although prevalent near GEO and only recently characterized with sufficient fidelity to incorporate in conjunction assessment [20]—are not considered in this study, this is an optimistic and conservative prediction of the actual congestion situation for GEO. On-orbit collision and fragmentation events are to be incorporated and addressed in future efforts.

4.3. Business as usual with perfect mitigation

The congestion forecasting performed thus far in this study has not yet addressed the influence of properly implemented mitigation measures for C1/C2 satellites reaching EOL. Classic mitigation for the GEO regime incorporates re-orbiting to graveyard disposal orbits at perigee altitudes above the GEO ring, factoring the protected GEO zone and area-to-mass-ratio of the satellite into the minimum altitude calculation [12,13,22], per the

[13] The baseline C1/C2 population in the 01/01/13 TLE set is also assigned this nominal lifetime (COSPAR designation provides launch year). Wegener et al. [27] and McKnight and Di Pentino [20] illustrate that the average design lifetime for GEO satellites has continued to increase since 1964, but extended lifetimes are not simulated here analysis.

[14] Chrystal et al. [5] and McKnight and Di Pentino [20] estimate that the probability of collision $\mathcal{P}_c$ at GEO is currently seven times larger near these gravitational wells.

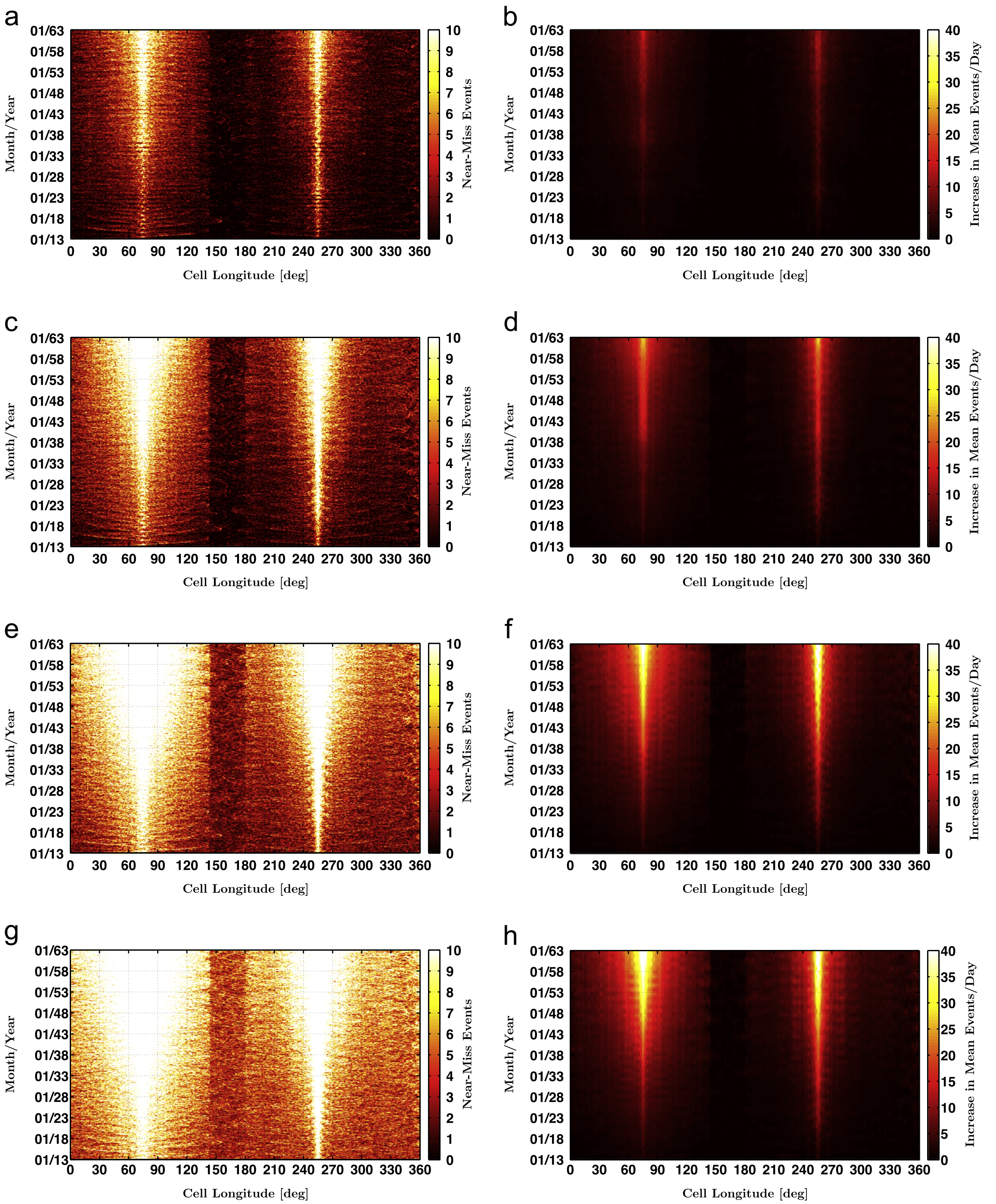

Fig. 6. 50-year GEO congestion forecasting with linearly increasing launch traffic model. (a) Near-miss forecast (50 km torus), (b) increase in near-misses (50 km torus), (c) near-miss forecast (100 km torus), (d) increase in near-misses (100 km torus), (e) near-miss forecast (300 km torus), (f) increase in near-misses (300 km torus), (g) near-miss forecast (700 km torus) and (h) increase in near-misses (700 km torus).

re-orbiting guidelines of the Inter-Agency Space Debris Coordination Committee (IADC) [11]. Though one might speculate that the IADC guidelines may increase the risk of derelict collision in the IADC debris orbit that could accumulate above GEO under these guidelines, Johnson [15] indicates that the variable amount of residual propellant at EOL has driven the wide variety of disposal orbits achieved in practice, such that the creation of a single "debris ring" is unlikely. To emphasize the importance of mitigation measures for GEO satellites, this study assumes "perfect" mitigation, in which a specified proportion of C1/C2 assets achieving EOL is successfully re-orbited to circular orbits at altitudes that *do not interfere* with the GEO radius in the prediction spans considered.

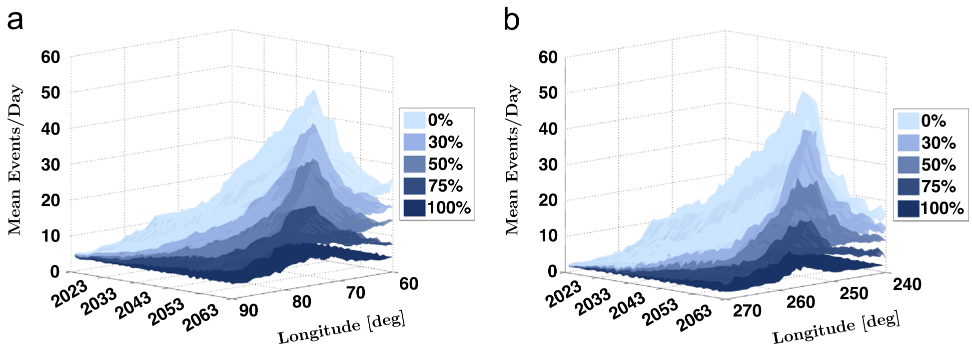

Fig. 7. Effect of perfect mitigation on congestion around gravity wells (300 km torus). Mitigation effect on (a) Eastern well and (b) Western well.

Fig. 7 illustrates the influence of this perfect mitigation on congestion in the neighborhoods of the Eastern and Western stable points, for 0% (equivalent to the "business-as-usual" scenario in Fig. 6), 30%, 50%, 75%, and 100% mitigation (equivalent to the "no future launches" scenario), for a GEO torus radius of 300 km. Fig. 7 portrays how the year-averaged number of near-miss events per day at a distance of 300 km increases over a 50-year period around these stable points for each of these mitigation scenarios. As the mitigation rate increases, the congestion peaks centered around these gravitational wells successively diminish to the level of the idealized "no future launches" traffic scenario. It is instructive to note that the case of 30% mitigation is the most representative of the rate actually carried out in the GEO regime during the 1997–2003 time frame [12,16]—of the 103 satellites that achieved EOL in this period, 34 were successfully re-orbited to IADC-compliant disposal orbits, 35 attempted re-orbiting, but resulted in orbits with insufficient perigee altitudes, and 34 were abandoned in libration orbits around the Eastern/Western stable points [12]. Low compliance may be attributed to (a) the sizable propellant cost for meeting the IADC re-orbit guidelines,[15] (b) the difficulty of estimating on-board propellant, and translating a computed re-orbit Δv into a required fuel mass [16], or (c) older, retiring satellites that were designed and built before establishment of the IADC guidelines, for which successful execution of the required maneuver was not often achievable [15].

Recently, however, Johnson [15] praises the strong support of the satellite operator community for preservation of the GEO ring. Of the 160 operational GEO satellites that achieved EOL in the period 2001–2010, approximately 80% successfully re-orbited to disposal orbits—of these satellites, 70% were transferred to orbits at least 200 km above GEO, and almost 50% achieved at least 300 km above GEO, fully compliant with the IADC re-orbit guidelines [15]. Even with the optimistic mitigation rate of 80%, however, Fig. 7 illustrates that the average number of near-miss events at 300 km in the vicinity of the gravitational wells will *double* by the year 2063. Since on-orbit collisions and fragmentation events are not considered in this study, the observed factor of two increase is a lower bound of true congestion increase likely to occur in this localized GEO environment. Although recent re-orbiting statistics are promising in that they suggest increased adherence to mitigation guidelines, and ultimately growing international desire to safeguard the GEO ring, Fig. 7 indicates that mitigation alone is not enough to stabilize the growing debris congestion at GEO with current re-orbiting success rates. To stabilize projected debris growth at GEO under current mitigation levels, active removal/remediation measures must be synthesized and implemented.

[15] Klinkrad [16] indicates that a typical re-orbiting maneuver requires a Δv of roughly 11 m/s, about 2.3% of the entire station-keeping budget for a 10-year operational lifetime.

5. Conclusion

Forecasting of localized debris congestion in the GEO environment is performed to quantify the frequency of near-miss events occurring for each longitude slot in the GEO ring. A reduced-fidelity propagator is implemented in parallel—in tandem with a GEO torus cell configuration and publicly-available TLE data—to simulate congestion in a "business-as-usual" launch traffic scenario, with and without mitigation at end-of-life. Results indicate that debris congestion in the vicinity of the two gravitational wells will become severe inasmuch as mitigation guidelines for this regime are not globally adhered to. Fortunately, a burgeoning desire to preserve GEO is reflected in the increasing numbers of satellite operators attempting re-orbit at end-of-life, but even under this optimistic, present-day mitigation rate of 80%, 300 km near-miss events in the vicinity of these gravitational wells will increase by a factor of two within 50 years. Ultimately, mitigation measures must be combined with active remediation in the GEO ring, to preserve the usefulness of this natural resource and driver for space development, and preclude a debris situation similar to that now sustained in the LEO environment.

Acknowledgments

The authors would like to acknowledge Brandon Jones and his TurboProp software [9], from which the integration routines employed in this research were obtained.

References

[1] P.V. Anderson, H. Schaub, Local orbital debris flux study in the geostationary ring, Adv. Space Res. 51 (June (12)) (2013) 2195–2206.
[2] J. Bendisch, K. Bunte, H. Klinkrad, H. Krag, C. Martin, H. Sdunnus, R. Walker, P. Wegener, C. Wiedemann, The master-2001 model, Adv. Space Res. 34 (2004) 959–968.
[3] M.M. Berry, L.M. Healy, Implementation of Gauss–Jackson integration for orbit propagation, J. Astronaut. Sci. 52 (July–September (3)) (2004) 331–357.
[4] V.A. Chobotov (Ed.), Orbital Mechanics, 3rd ed. American Institute of Aeronautics and Astronautics, Inc, 2002.
[5] P. Chrystal, D. McKnight, P. Meredith, Space Debris: On Collision Course for Insurers? Technical Reports, Swiss Reinsurance Company Ltd., 2011.
[6] H. Curtis, Orbital Mechanics for Engineering Students, Elsevier Butterworth-Heinemann, 2005.
[7] T. Flohrer, Classification of Geosynchronous Objects: Issue 14, Technical Report 1, European Space Operations Centre, February 2012.
[8] T. Flohrer, H. Krag, H. Klinkrad, Assessment and categorization of tle orbit errors for the us ssn catalogue, in: Proceedings of the 2008 Advanced Maui Optical and Space Surveillance Technologies Conference, September 2008.
[9] K. Hill, B.A. Jones, TurboProp Version 4.0, Colorado Center for Astrodynamics Research, University of Colorado at Boulder, May 2009.
[10] F.R. Hoots, R.L. Roehrich, Spacetrack Report No. 3, Models for Propagation of Norad Element Sets, Technical Report, Office of Astrodynamics, Aerospace Defense Center, December 1980.
[11] IADC/WG4, Iadc Space Debris Mitigation Guidelines, Technical Reports, IADC, September 2007.
[12] R. Jehn, V. Agapov, C. Hernandez, The situation in the geostationary ring, Adv. Space Res. 35 (2005) 1318–1327.
[13] R. Jehn, C. Hernandez, International practices to protect the geostationary ring, Space Debris 1 (2001) 221–233.
[14] N. Johnson, Protecting the geo environment: policies and practices, Space Policy 15 (1999) 127–135.
[15] N.L. Johnson, A new look at the geo and near-geo regimes: operations, disposals, and debris, Acta Astronaut. 80 (June) (2012) 82–88.
[16] H. Klinkrad, Space Debris: Models and Risk Analysis, Praxis Publishing, 2006.
[17] H. Lewis, G. Swinerd, N. Williams, G. Gittins, Damage: a dedicated geo debris model framework, in: Proceedings of the 3rd European Conference on Space Debris, vol. 1, ESA Publications Division, March 2001.
[18] J.-C. Liou, D.T. Hall, P.H. Krisko, J.N. Opiela, Legend: a three-dimensional leo-to-geo debris evolutionary model, Adv. Space Res. 34 (2004) 981–986.
[19] K. Luu, C. Sabol, Effects of Perturbations on Space Debris in Supersynchronous Storage Orbits, Technical Reports, Air Force Research Laboratory, October 1998.
[20] D.S. McKnight, F.R. Di Pentino, New insights on the orbital debris collision hazard at geo, Acta Astronaut. 85 (2013) 73–82.
[21] O. Montenbruck, E. Gill, Satellite Orbits: Models, Methods, Applications, Springer, 2000.
[22] NASA, Process for limiting orbital debris, NASA-STD-8719.14 Change 4, National Aeronautics and Space Administration, September 2009.
[23] H. Schaub, L.E.Z. Jasper, Circular orbit radius control using electrostatic actuation for 2-craft configurations, in: Proceedings of the 2011 AAS/AIAA Astrodynamics Specialist Conference, August 2011.
[24] USNO, UKHO, The Astronomical Almanac for the Year 2013, U.S. Nautical Almanac Office with Her Majesty's Nautical Almanac Office, 2013.
[25] D. Vallado, Fundamentals of Astrodynamics and Applications, 3rd ed. Microcosm Press, 2007.
[26] D.A. Vallado, P. Crawford, R. Hujsak, T.S. Kelso, Revisiting spacetrack report no. 3: revision 2, in: Proceedings of the 2006 AIAA/AAS Astrodynamics Specialist Conference, August 2006.
[27] P. Wegener, J. Bendisch, H. Krag, M. Oswald, S. Stabroth, Population evolution in the geo vicinity, Adv. Space Res. 34 (2004) 1171–1176.
[28] T. Yasaka, T. Hanada, H. Hirayama, Geo debris environment: a model to forecast the next 100 years, Adv. Space Res. 23 (1) (1999) 191–199.